JACS
JOURNAL OF THE AMERICAN CHEMICAL SOCIETY
pubs.acs.org/JACS
Article

^{3}d-d Excited States of Ni(II) Complexes Relevant to Photoredox Catalysis: Spectroscopic Identification and Mechanistic Implications

Stephen I. Ting, Sofia Garakyaraghi, Chelsea M. Taliaferro, Benjamin J. Shields, Gregory D. Scholes, Felix N. Castellano, and Abigail G. Doyle*

Cite This: J. Am. Chem. Soc. 2020, 142, 5800−5810
Read Online
ACCESS | Metrics & More | Article Recommendations | Supporting Information

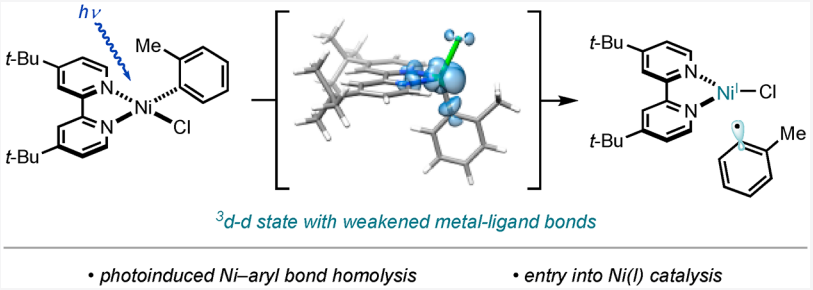

ABSTRACT: Synthetic organic chemistry has seen major advances due to the merger of nickel and photoredox catalysis. A growing number of Ni-photoredox reactions are proposed to involve generation of excited nickel species, sometimes even in the absence of a photoredox catalyst. To gain insights about these excited states, two of our groups previously studied the photophysics of Ni($^{t\text{-Bu}}$bpy)(*o*-Tol)Cl, which is representative of proposed intermediates in many Ni-photoredox reactions. This complex was found to have a long-lived excited state (τ = 4 ns), which was computationally assigned as a metal-to-ligand charge transfer (MLCT) state with an energy of 1.6 eV (38 kcal/mol). This work evaluates the computational assignment experimentally using a series of related complexes. Ultrafast UV−Vis and mid-IR transient absorption data suggest that a MLCT state is generated initially upon excitation but decays to a long-lived state that is ^{3}d-d rather than ^{3}MLCT in character. Dynamic *cis*,*trans*-isomerization of the square planar complexes was observed in the dark using ^{1}H NMR techniques, supporting that this ^{3}d-d state is tetrahedral and accessible at ambient temperature. Through a combination of transient absorption and NMR studies, the ^{3}d-d state was determined to lie ∼0.5 eV (12 kcal/mol) above the ground state. Because the ^{3}d-d state features a weak Ni−aryl bond, the excited Ni(II) complexes can undergo Ni homolysis to generate aryl radicals and Ni(I), both of which are supported experimentally. Thus, photoinduced Ni−aryl homolysis offers a novel mechanism of initiating catalysis by Ni(I).

1. INTRODUCTION

In recent years, synthetic organic chemistry has seen widespread activity in the development of light-driven reactions. A particularly rich area of research combines photoredox catalysis with nickel catalysis.[1,2] Often referred to as Ni-photoredox, this combination enhances Ni cross-coupling by leveraging the ability of photoredox catalysis to generate reactive intermediates.[3−6] Advances in Ni-photoredox have enabled many C−C and C−heteroatom cross-couplings that pose major challenges for Ni catalysis on its own.[1,2]

Ni-photoredox canonically involves electron transfers between the photocatalyst and other reaction components to generate reactive species.[1,2] However, an increasing number of reactions are proposed to form excited Ni species by energy transfer with an exogenous photocatalyst (Figure 1A).[7−9] These excited Ni species have been invoked to undergo a variety of processes that ultimately enable product formation. For instance, excited Ni(II) complexes have been proposed to undergo Ni−Br bond homolysis,[7] C−O reductive elimination,[8] and ligand-to-metal charge transfer (Figure 1A).[9] The importance of excited Ni species becomes even more clear upon considering that light can promote Ni catalysis in the absence of an exogenous photocatalyst. This has been demonstrated by a light-promoted C−O coupling from two of our groups (Figure 1B)[10] and contributions from others of an enantioselective Giese reaction[11] and a C−N coupling.[12]

While the above examples demonstrate the importance of excited Ni complexes in Ni-photoredox, these excited states have been sparingly investigated. Most Ni-photoredox reactions use 2,2′-bipyridine (bpy) derivatives or other bidentate nitrogen-based ligands. In contrast, most photophysical studies

Received: January 20, 2020
Published: March 9, 2020

https://dx.doi.org/10.1021/jacs.0c00781
J. Am. Chem. Soc. 2020, 142, 5800−5810

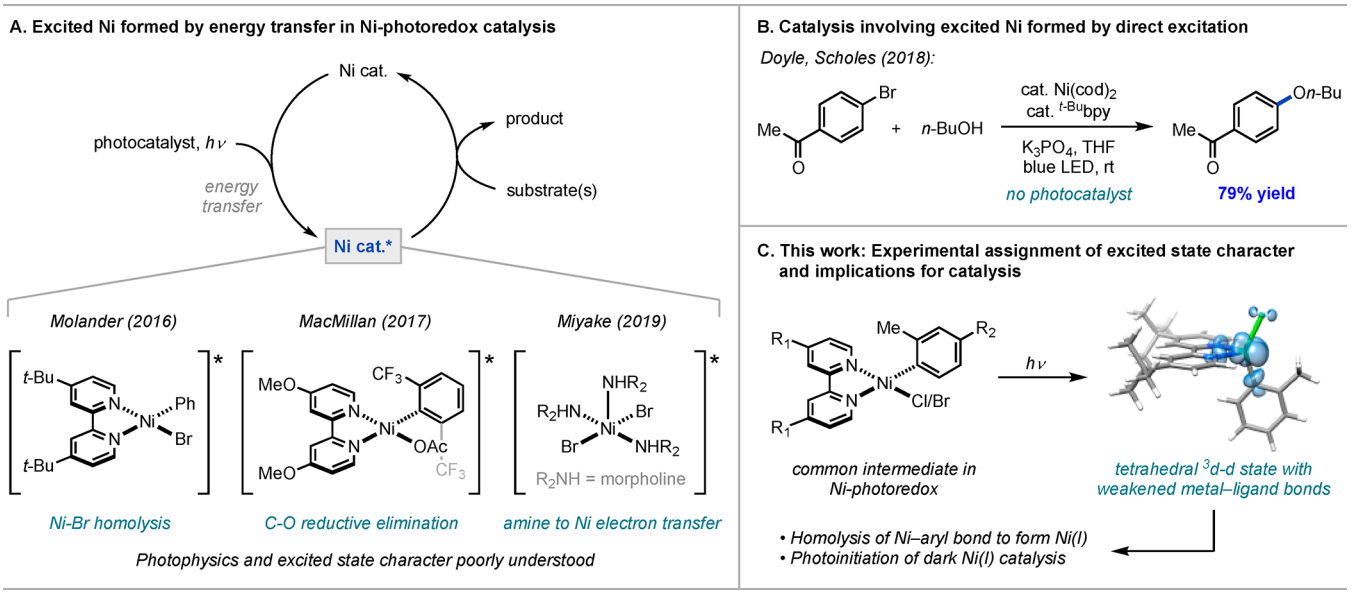

Figure 1. Ni(II) excited states relevant to Ni-photoredox catalysis.

of Ni complexes involve complexes bearing macrocyclic ligands.[13−18] Therefore, we sought to characterize the excited states of Ni complexes relevant to Ni-photoredox reactions.

The nature of an excited state has major implications for its reactivity and is thus critical to establish. As seen in many octahedral d^6 complexes (e.g., $[Ru(bpy)_3]^{2+}$), metal-to-ligand charge transfer (MLCT) states are often long lived (~1 μs) and well suited for bimolecular electron transfer.[19] In contrast, d-d states of the same complexes tend to undergo rapid nonradiative decay.[20−22] This is due to occupation of d orbitals that are σ-antibonding with the ligands; the resulting structural distortion horizontally displaces the excited state energy surface from the ground state surface, creating a low-energy surface crossing to return to the ground state. Occupation of metal−ligand σ-antibonding orbitals also promotes metal−ligand bond cleavage, further highlighting the distinct properties of different excited states. Assigning the excited states of Ni complexes relevant to Ni-photoredox would enable a better understanding of their role in this synthetic context.

In an initial investigation, two of our groups studied Ni($^{t\text{-Bu}}$bpy)(*o*-Tol)Cl (**1**$^{t\text{-Bu}}$), since complexes of this type are believed to be intermediates in many Ni-photoredox reactions (*o*-Tol = *o*-tolyl).[10] This complex was found to feature a MLCT absorption band and forms a long-lived excited state upon excitation (τ = 4 ns). This nonemissive excited state was observed by transient absorption (TA) spectroscopy and computationally assigned as a ^{3}MLCT state. This assignment was striking given that first-row transition metal complexes commonly relax into d-d rather than MLCT states.[23−25] We thus sought to evaluate this computational ^{3}MLCT assignment experimentally, considering the alternative possibility of a d-d state. Data from a series of related derivatives support that a MLCT state is generated initially, but that it evolves in ~5−10 ps to a long-lived ^{3}d-d state with an energy of ~0.5 eV (Figure 1C). On the basis of computational and organometallic studies, we propose that the ^{3}d-d state provides a pathway for photoinduced Ni−aryl bond homolysis, generating Ni(I) species that may be responsible for catalysis in reactions proceeding via excited Ni(II). This constitutes a novel mechanism for catalyst initiation and provides a mechanistic basis for developing light-driven cross-coupling reactions that do not require exogenous photosensitizers.

2. RESULTS AND DISCUSSION

2.1. Photophysical Studies. To facilitate excited state assignment, several complexes of the type Ni(^{R}bpy)(Ar)X were prepared to enable determination of structure−activity relationships (Figure 2; Ar = aryl, X = halide). In the bipyridine series

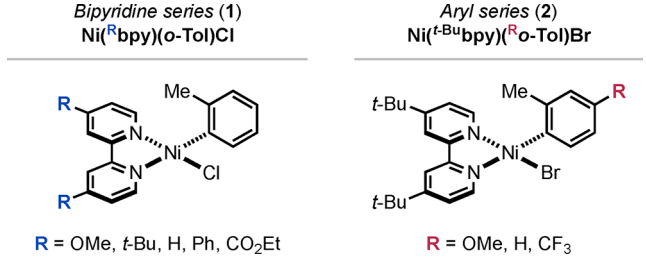

Figure 2. Ni(II) complexes studied in this work.

(**1**), the bpy ligand was modified with various electron-donating or -withdrawing groups at the 4,4′-positions (OMe, *t*-Bu, H, Ph, CO_2Et). In the aryl series (**2**), similar substituents were introduced at the 4-position of the aryl ligand (OMe, H, CF_3). The two series differ in the halide on Ni (Cl vs Br), with the aryl series containing bromides for ease of synthesis (see Supporting Information).

2.1.1. UV−Vis Absorption Spectroscopy. While the ultimate goal was to characterize the long-lived excited state of the Ni complexes, electronic absorption spectroscopy provides insights into the excited state generated at the moment of excitation. The electronic absorption spectrum of Ni($^{t\text{-Bu}}$bpy)(*o*-Tol)Cl (**1**$^{t\text{-Bu}}$) was previously assigned by time-dependent density functional theory (TD-DFT) calculations to comprise a $^{t\text{-Bu}}$bpy ligand-centered (π,π^*) transition in the UV and a MLCT transition in the visible region.[10] The (π,π^*) transition was previously verified experimentally by comparison to the spectrum of the free ligand, while the MLCT assignment was made computationally. To experimentally support the prior MLCT assignment, electronic absorption spectra were recorded in the present

https://dx.doi.org/10.1021/jacs.0c00781
J. Am. Chem. Soc. 2020, 142, 5800−5810

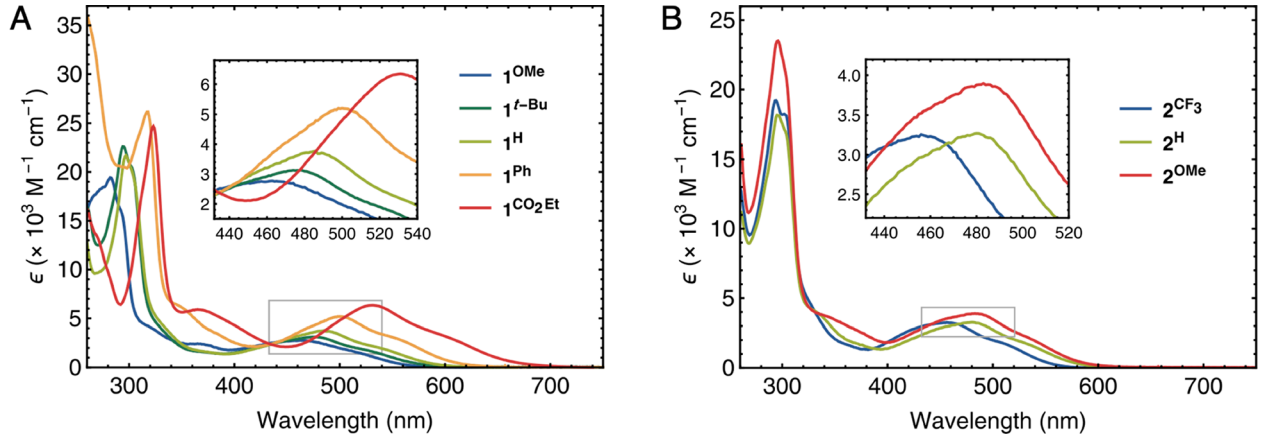

Figure 3. UV−Vis absorption spectra in THF of (A) the bipyridine series **1**, Ni(^{R}bpy)(*o*-Tol)Cl and (B) the aryl series **2**, Ni($^{t\text{-Bu}}$bpy)(^{R}*o*-Tol)Br. Insets show an expanded view of the regions highlighted in gray boxes. Note the difference in vertical scales.

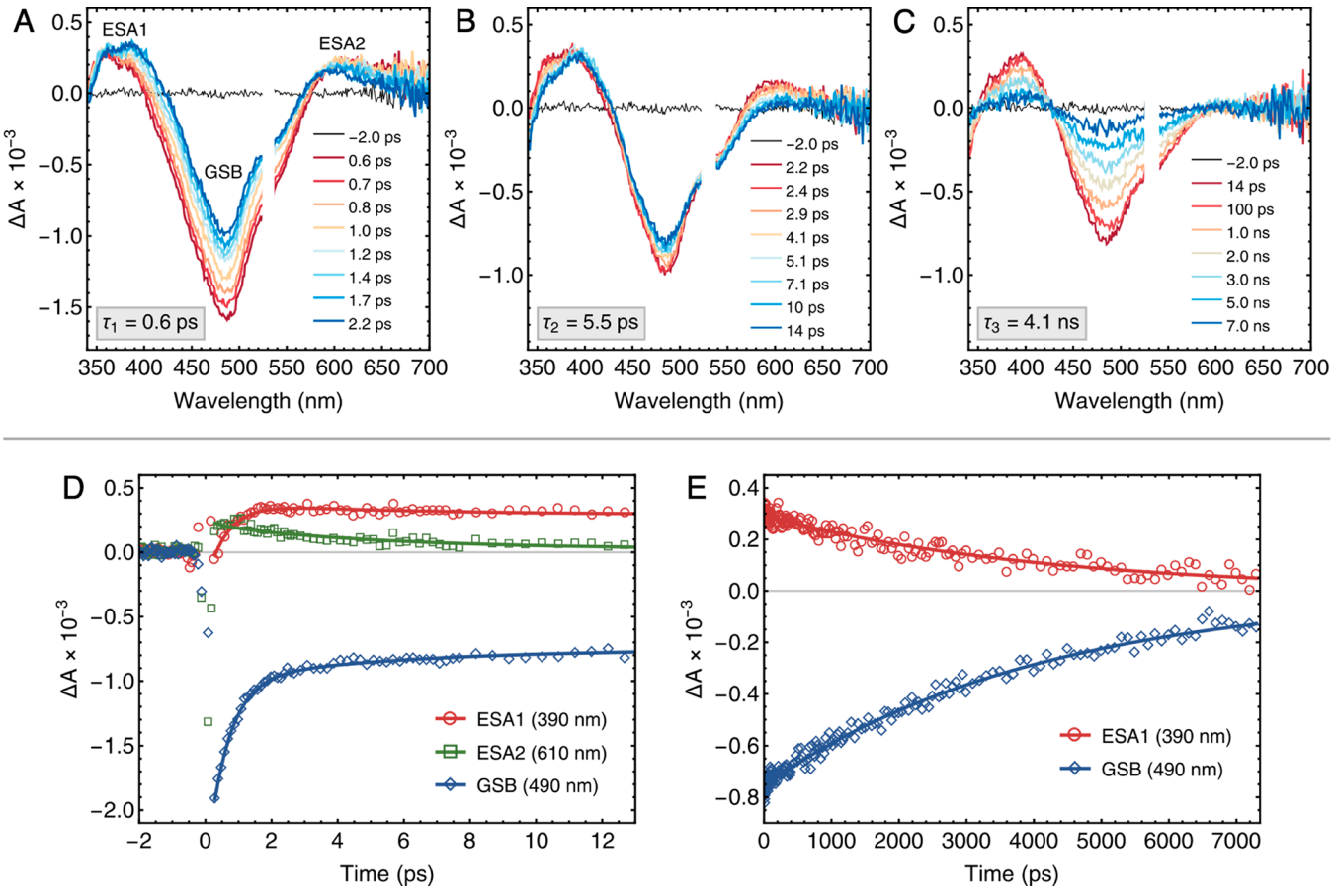

Figure 4. Subpicosecond TA difference spectra of Ni(bpy)(*o*-Tol)Cl (**1**^{H}) in deoxygenated THF upon 530 nm pulsed laser excitation (0.500 μJ per pulse, 100 fs fwhm) with the following delay times: (A) 0.6−2.2, (B) 2.2−14, and (C) 14−7000 ps. Laser scatter surrounding the excitation wavelength has been removed for clarity. Bottom panels show experimental TA kinetics along with global fits between the following delay times: (D) between −2 and 13 ps, (E) between 13 and 7300 ps. ESA = excited state absorption. GSB = ground state bleach.

study for both series of complexes. If the transition were MLCT, a bathochromic shift would be expected as the bpy π^* is systematically lowered through conjugation or substitution with electron-withdrawing groups (^{OMe}bpy → ^{CO_2Et}bpy). This is indeed observed, providing evidence that the electron is promoted into the bpy π^* (Figure 3A). Similarly, a bathochromic shift would be expected as the Ni-centered orbitals are raised by a more donating aryl ligand (^{CF_3}*o*-Tol → ^{OMe}*o*-Tol). This is also observed, supporting that the electron emanates from a HOMO largely localized on Ni (Figure 3B).

The MLCT assignment is further supported by the magnitudes of the shifts as the substituents are varied. Specifically, varying the aryl ligand leads to a smaller shift of the visible absorption band (1180 cm^{-1}) compared to when the bpy ligand is varied (2810 cm^{-1}). This is despite the substituents in the aryl ligand spanning a greater range of electronic properties than the substituents in the bpy series (aryl series has

https://dx.doi.org/10.1021/jacs.0c00781
J. Am. Chem. Soc. 2020, 142, 5800−5810

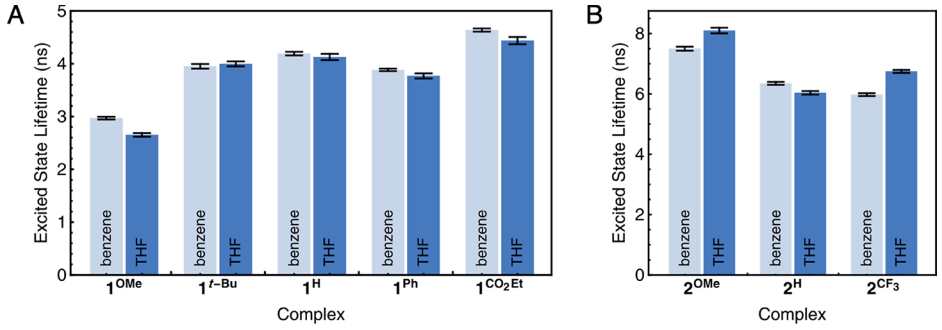

Figure 5. Excited state lifetimes measured by TA upon MLCT excitation in deoxygenated solvent. (A) Bipyridine series **1**, Ni(^{R}bpy)(*o*-Tol)Cl. (B) Aryl series **2**, Ni($^{t\text{-Bu}}$bpy)(^{R}*o*-Tol)Br. Kinetic data for all complexes is tabulated in Tables S2 and S3. Details regarding excitation wavelength and power are given in the Supporting Information.

CF_3, σ_p 0.54; bpy series has CO_2Et, σ_p 0.45).[26,27] This provides evidence that the promoted electron does not originate from the aryl ligand itself but rather from the Ni center which would be less directly affected by substituents on the aryl ligand. The assignment of the visible band as a MLCT transition is further substantiated by the magnitudes of the extinction coefficients. It is known that extinction coefficients for charge transfer transitions increase as the promoted electron is transferred over a longer distance.[28,29] Consistent with this, the variants bearing the more extensively conjugated ^{Ph}bpy and ^{CO_2Et}bpy ligands have higher extinction coefficients compared to all other derivatives (Figure 3, Table S1). Overall, the combined UV−Vis data support the prior computational assignment of a low-energy visible MLCT transition, indicating that a MLCT state is initially generated upon excitation of this band.

2.1.2. Transient Absorption (TA) Spectroscopy. In order to study excited states after their initial photoactivation, transient absorption (TA) spectroscopy was employed. The complexes Ni(^{R}bpy)(Ar)X afford similar TA difference spectra featuring comparable dynamics (the biggest difference is a shift in wavelength, reflecting the ground state UV−Vis spectra). Thus, the simplest complex in the family, Ni(bpy)(*o*-Tol)Cl (**1^{H}**), is discussed as a representative example.

Upon MLCT excitation in THF, a transient spectrum is initially generated that undergoes two distinct spectral changes before decaying to the baseline. The transient spectrum observed 0.6 ps after excitation is shown as the red curve in Figure 4A and exhibits two excited state absorptions (ESA1, ESA2) surrounding a ground state bleach (GSB). The positions of ESA1 and ESA2 (370 and 610 nm, respectively) are close to the absorptions of the bpy radical anion (397 and 582 nm in DMF).[30] This enables assignment of a MLCT state at early times, as the MLCT state formally contains a reduced bpy ligand. Moreover, ESA1 and ESA2 are reminiscent of excited state absorptions observed in the TA difference spectrum of $[Ru(bpy)_3]^{2+}$ (~370 nm and a broad feature from 500 to 650+ nm).[31]

Between 0.6 and 2 ps, the spectral changes are dominated by decay of GSB. This is accompanied by the broadening of ESA1 on its red edge and ESA2 on its blue edge, as well as a decay on the red edge of ESA2. Although somewhat altered in position and shape, ESA1 and ESA2 still closely match the absorptions of bpy$^{\bullet-}$, indicating that the excited state remains MLCT in character. Based on the blue shift of ESA2, we assign this time constant to vibrational relaxation, although the assignment of this specific time constant is of minor importance to the current work.[32,33]

More important is the second spectral change that occurs between ~2 and 15 ps, shown in Figure 4B. During this time, ESA1 narrows on its blue edge, GSB reduces in intensity, and ESA2 decays essentially to baseline. This yields a much longer lived excited state that returns to the ground state on a nanosecond time scale, shown by the symmetric decay to baseline in Figure 4C. Most notable about the evolution between ~2 and 15 ps is the loss of ESA2 (Figure 4B and 4D). Given that bpy$^{\bullet-}$ is associated with absorptions corresponding to both ESA1 and ESA2, the loss of ESA2 suggests that the excited state no longer contains a reduced bpy ligand. This likely reflects the evolution of the MLCT state to an excited state of different character, such as a d-d state. While this could argue against the previous MLCT assignment, the data are not conclusive as ESA2 remains present at long times for most complexes, albeit at greatly reduced intensity (see Supporting Information). While density functional theory (DFT) calculations indicate that a ^{3}d-d state would account for the persistence of ESA1 at long times, additional experiments were necessary to assign the long-lived excited state (Figure S50).[34]

2.1.2.1. Substituent Effects. Aiming to assign the longest-lived component, the dependence of its lifetime on substituents was investigated. If the longest-lived component was MLCT, its lifetime could be systematically varied as the MLCT energy is changed by substituents on the complex (see UV−Vis Absorption Spectroscopy). Drawing from knowledge of photosensitizers related to $[Ru(bpy)_3]^{2+}$, changing the MLCT energy can influence lifetimes in two main ways.[19,22] (1) The energetic separation from faster decay channels (e.g., d-d states) could be changed, altering the contribution of these channels to MLCT decay. For Ru(II) polypyridines, lowering the MLCT energy increases the energy separation from higher lying d-d states, causing slower nonradiative decay. (2) The energy gap between the MLCT state and the ground state could be changed, affecting the rate of direct MLCT decay, with lower MLCT energies leading to faster nonradiative decay (energy gap law). These factors oppose each other, and either factor can be dominant. As exemplified by Ru(II) terpyridines, factor (1) dominates when d-d state involvement is significant, and factor (2) dominates when the MLCT energy becomes close enough to the ground state energy.[22] For the Ni(II) complexes in the present study, we thus expected that the lifetime would depend on the MLCT energy in one of these two ways, provided that the long-lived component was in fact MLCT in character.

Excited state lifetimes for both the bpy series (**1**) and the aryl series (**2**) were determined through monoexponential fits of the

https://dx.doi.org/10.1021/jacs.0c00781
J. Am. Chem. Soc. 2020, 142, 5800−5810

ground state bleach after 250 ps. The obtained lifetimes were found to be quite insensitive to the nature of the substituents, despite the broad range of their electron-donating or -withdrawing abilities (Figures 5 and S29−32). With few exceptions, the lifetime is roughly constant at around 4 ns for the bpy series and around 7 ns for the aryl series (the difference being due to Cl vs Br as the halide for reasons that are unclear). The relatively constant lifetimes (within a factor of 2 for each series) contrast with trends for known MLCT states, whose lifetimes can span orders of magnitude depending on the MLCT energy.[22,35] This calls into question the previous computational assignment of a MLCT state. However, the lifetime data alone are insufficient to rule out a long-lived MLCT state. It is possible that the two factors mentioned above could offset each other to give little effect. That is, lowering a MLCT state could reduce access to higher energy decay channels while also accelerating direct decay from the MLCT state. Thus, additional data were needed to assign the longest-lived state.

2.1.2.2. Solvent Effects. To gain more information about the complexes Ni(^{R}bpy)(Ar)X, we recognized that the photophysics could be affected by solvent. If the long-lived component were MLCT, solvent polarity would modify the energy of the charge-separated MLCT state, changing the lifetime as discussed in the previous section. However, our survey of substituent effects showed that changing the MLCT energy had no major effect on the lifetime (*vide supra*). We thus reasoned that any solvent effects would be due to the Lewis basicity rather than the polarity of the solvent.

The Lewis basicity of the solvent affects excited state ligand binding, a well-known phenomenon that can dramatically alter the excited state lifetimes of metal complexes.[13,14,36−41] For d^8 metals, the binding results from creation of a d_{z^2} hole by electron promotion. Interactions of ligands with this orbital then become net bonding, analogous to how net bonding is exhibited in He_2^+ but not He_2. The effect resulting from ligand binding can vary depending on the system. In many cases, ligand binding dramatically shortens excited state lifetimes, as seen for the ^{3}MLCT states of Pt(II) terpyridines[36,37] and Cu(I) phenanthrolines.[38−40] In other cases, ligand binding leads to significant increases in lifetimes, as is known for ^{3}d-d states of Ni(II) porphyrins and phthalocyanines.[13,14,41] From these studies, binding of pyridine to excited Ni(II) occurs in ∼100−450 ps, well within the nanosecond lifetimes of complexes in the present study.

To assess whether excited state solvent coordination occurs for Ni(^{R}bpy)(Ar)X, excited state lifetimes of all variants were measured in benzene and THF. These solvents differ significantly in Lewis basicity, as indicated by their Gutmann donor numbers (DN; 0.1 for benzene, 20.0 for THF).[42,43] More coordinating solvents were not employed, as they displace the halide in the ground state.[44,45] Experimentally, it was found that the solvent has little effect on the lifetime, suggesting there is no solvent coordination to Ni in the excited state (Figure 5, light vs dark bars).[46] This was rather surprising since excited state ligand binding is known for both MLCT and d-d states, only requiring that a d_{z^2} hole is created by photoexcitation.

A possible explanation for the lack of solvent effect lies in the geometry. The Pt(II) terpyridines and Ni(II) porphyrins mentioned above are constrained to planar geometries by virtue of a tridentate or macrocyclic ligand. Thus, the axial faces of the metal are always exposed to solvent. In contrast, structures of type Ni(^{R}bpy)(Ar)X have the possibility of distorting to a tetrahedral structure, reducing access of solvent to the metal center (Figure 6). Such a tetrahedral structure corresponds to a d-d state, reflecting movement of ligands out of the square plane due to electron promotion into the $d_{x^2-y^2}$ orbital.

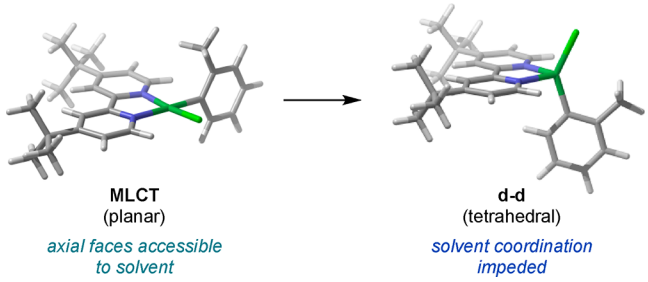

Figure 6. Excited state structural change. Structures shown were computed by DFT (M06/TZVP//B3LYP/TZVP).

Indeed, DFT calculations located ^{3}d-d states with tetrahedral geometries (Figures 6, S49 and S57). The ^{3}d-d states of Pt(II) complexes are also believed to be tetrahedral.[47] Such ^{3}d-d states correspond to the ground state of high-spin, 4-coordinate Ni(II) complexes,[48] which resist ligand binding and only undergo associative ligand substitution through an equilibrium with a square planar singlet state.[49,50] This supports the possibility that a tetrahedral ^{3}d-d state could account for the lack of solvent effect. However, we note that ligation of excited Ni(II) has historically been studied mostly with pyridine (DN 33.1), which is far more Lewis basic than the THF employed in the present study. Moreover, solvent coordination is believed not to be operative in some cases.[15,51] Thus, while the lack of solvent effect suggests a long-lived ^{3}d-d state, more direct evidence was needed.

2.1.3. Time-Resolved Infrared (TRIR) Spectroscopy. To provide more direct evidence that the longest lived component may be ^{3}d-d in nature, time-resolved infrared (TRIR) spectroscopy was employed. This technique allows the observation of IR difference spectra at various time points after excitation. We elected to study Ni(^{CO_2Et}bpy)(*o*-Tol)Cl (**1**^{CO_2Et}) as the bpy ligand contains carbonyl handles valuable for IR spectroscopy. Monitoring the C═O stretching frequency ($\nu_{C=O}$) after excitation provides a direct readout of bpy ligand reduction, which would be observed for a MLCT state but not a d-d state. This would then allow a definitive assignment of whether excited states are MLCT or not.

At short delay times (<10 ps) after excitation, a bleach of the ground state IR absorption (GSB) is seen, along with growth of an ESA at reduced frequencies (∼1725 cm^{-1}, Figure 7A). This shift to lower $\nu_{C=O}$ is consistent with a weakened C═O bond resulting from a reduced bpy ligand in a MLCT state. This is in accord with the UV−Vis transient absorption data, which show excited state absorptions at early times that match known absorptions of the reduced bpy ligand (Figure 4A and 4B).

At longer delay times (>10 ps), the C═O stretch of the excited state shifts to higher frequency than that of the ground state. As shown in Figure 7A and 7B, the initial ESA at lower $\nu_{C=O}$ (1727 cm^{-1}) decays while a new ESA grows in at higher $\nu_{C=O}$ (1735 cm^{-1}). This evolution occurs with a time constant of ∼9 ps, and the resulting signal decays to baseline with a time constant of ∼4 ns (Figure S34). The increased $\nu_{C=O}$ observed after ∼10 ps is inconsistent with reduction of the bpy ligand and definitively rules out a MLCT assignment for the longest-lived component. Rather, it is consistent with a d-d state, as the weaker (and thus longer) metal−ligand bonds would diminish

https://dx.doi.org/10.1021/jacs.0c00781
J. Am. Chem. Soc. 2020, 142, 5800−5810

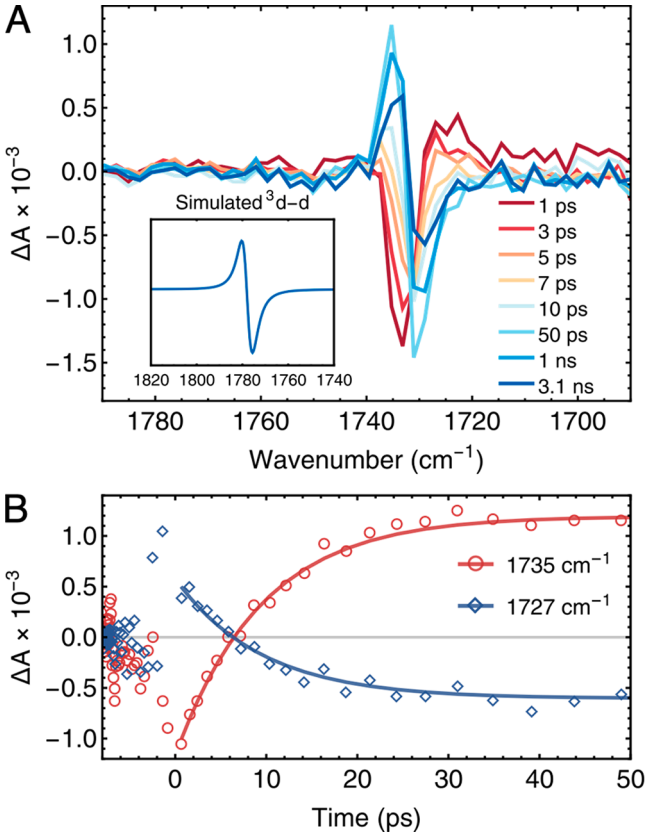

Figure 7. (A) Experimental TRIR difference spectra of Ni(^{CO_2Et}bpy)(*o*-Tol)Cl (**1**^{CO_2Et}) in deoxygenated THF upon 610 nm pulsed laser excitation (3 μJ per pulse, 100 fs fwhm). (Inset) DFT-calculated IR difference spectrum for the tetrahedral ^{3}d-d state of **1**^{CO_2Et}. (B) TRIR kinetics up to a delay time of 50 ps, shown along with global fits. τ_1 = 9.5 ps, τ_2 = 4.3 ns.

π-backbonding into the ^{CO_2Et}bpy ligand. This assignment is supported by DFT, which predicts a qualitatively similar TRIR difference spectrum for a ^{3}d-d state with a tetrahedral geometry (Figure 7A, inset). Additionally, the 9 ps time constant for d-d state formation reasonably matches the time constant associated with loss of a reduced ligand signature in UV−Vis TA (8 ps for this complex, Table S3). This suggests that the same process is observed in both experiments. Taken together, this information provides strong evidence that the ∼5−10 ps time constant corresponds to evolution from MLCT to a long-lived state that is ^{3}d-d in character.

2.1.4. 2D Exchange Spectroscopy (EXSY). DFT calculations predicted that the lowest excited state (^{3}d-d) is low enough in energy to be thermally accessible at room temperature (10.8 kcal/mol, *vide infra*). Given that the ^{3}d-d state is tetrahedral (based on DFT and known high-spin Ni(II) complexes), population of this state would provide a mechanism for *cis,trans*-isomerization without light. The effect would be to exchange whether a given pyridine of the bpy ligand is *cis* to the aryl group or the halide. Observation of this exchange without irradiation would provide further evidence of a tetrahedral ^{3}d-d state and confirm its energetic accessibility. This exchange was assessed by using ^{1}H NMR techniques to study Ni($^{t\text{-Bu}}$bpy)(*o*-Tol)Cl (**1**$^{t\text{-Bu}}$). Each pyridine contributes a *t*-Bu singlet that is separated from other ^{1}H NMR resonances, rendering this system well suited for study.

The two *t*-Bu groups give rise to two NMR signals at room temperature, indicating that any exchange must be relatively slow. Thus, exchange was probed by 2D exchange spectroscopy (EXSY), an NMR technique that shows cross peaks between protons that undergo exchange.[52] These cross peaks are indeed observed for the *t*-Bu groups in Ni($^{t\text{-Bu}}$bpy)(*o*-Tol)Cl (**1**$^{t\text{-Bu}}$), which were determined to undergo exchange with a rate of 0.62 ± 0.01 s^{-1} (Figures 8 and S42). This provides further evidence

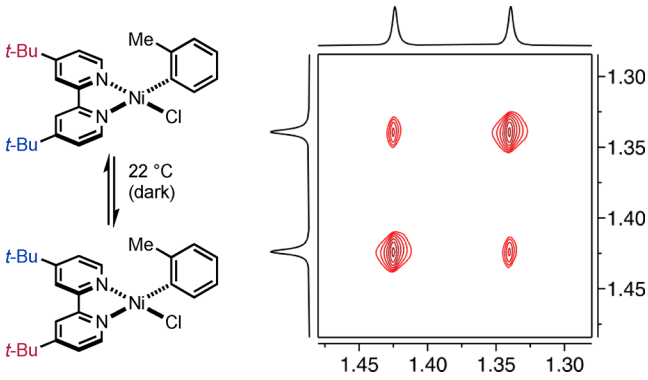

Figure 8. 2D EXSY spectrum of Ni($^{t\text{-Bu}}$bpy)(*o*-Tol)Cl (**1**$^{t\text{-Bu}}$) in THF-d_8 at 22 °C (t_m = 150 ms). The peaks shown are the *t*-Bu resonances.

for a tetrahedral ^{3}d-d state, as twisting of the $^{t\text{-Bu}}$bpy ligand proceeds through a tetrahedral structure. This unimolecular twisting mechanism is supported by a near-zero value of $\Delta S^{\ddagger}$ (−2.1 ± 0.6 eu) and a similar exchange rate with a more strongly chelating phenanthroline ligand, which argues against partial dissociation of the bidentate ligand (Figures S47 and S48). Moreover, photoisomerization of isoelectronic Pt(II) complexes via ^{3}d-d states has been shown to occur through a unimolecular bond rotation.[47]

The tetrahedral geometry of the ^{3}d-d state has several consequences. First, we suspect that changes between tetrahedral and planar geometries may intimately affect the rate of ground state recovery in ways that we currently do not understand. Second, the thermal accessibility of this tetrahedral state indicates that Ni(II) complexes may be more fluxional than is generally appreciated. The dynamic *cis,trans*-isomerization observed by EXSY may have broad implications for nickel catalysis, particularly where isomerization at Ni could influence regio-, diastereo-, and/or enantioselectivity.

2.1.5. Determination of Excited State Energy. Since 2D EXSY supported that a tetrahedral ^{3}d-d state is accessible at room temperature, we sought to experimentally determine the ^{3}d-d energy. Since the complexes are nonemissive and redox bracketing was challenging, we capitalized on the fact that EXSY provided the rate constant for *cis,trans*-isomerization. Assuming the rate of isomerization equals the rate of accessing the tetrahedral ^{3}d-d state, the rate of thermally accessing the ^{3}d-d state from the ground state is then known (Figure 9). The rate of the reverse process corresponds to ^{3}d-d state decay and is also known (from TA). The ratio of forward/reverse rate constants then gives K_{eq} and thus $\Delta G°$. Following this procedure, the ^{3}d-d state was determined to be 0.50 eV (12 kcal/mol) above the ground state. Thus, the combination of EXSY and TA enabled an experimental determination of the ^{3}d-d energy, circumventing the problem of measuring emission from these nonemissive complexes.

https://dx.doi.org/10.1021/jacs.0c00781
J. Am. Chem. Soc. 2020, 142, 5800−5810

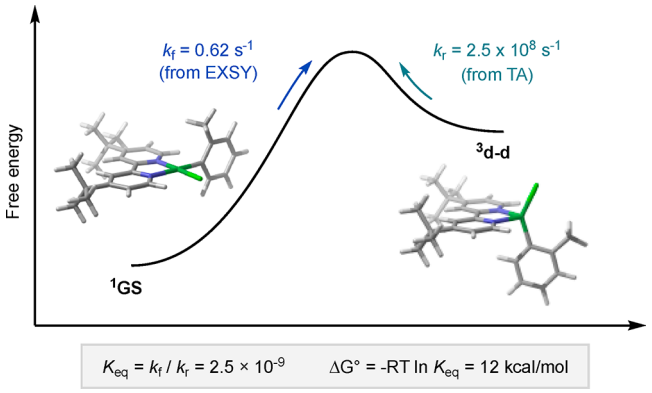

Figure 9. Experimental determination of the ^{3}d-d energy for Ni($^{t\text{-Bu}}$bpy)(*o*-Tol)Cl (**1**$^{t\text{-Bu}}$). Structures shown were calculated by DFT (M06/TZVP//B3LYP/TZVP).

We note that combining EXSY and TA data requires the assumption that the same ^{3}d-d state is accessed in both experiments. We believe this assumption is reasonable since the ^{3}d-d state is the lowest excited state identified by density functional theory (DFT). Calculations at the M06/TZVP//B3LYP/TZVP level of theory reproduce the experimental ^{3}d-d energy (computed 10.8 kcal/mol), showing that the ^{3}d-d state lies much lower than the previously computed ^{3}MLCT state (1.6 eV or 38 kcal/mol).[10] High-level calculations on related complexes have also found d-d states to be significantly lower in energy than MLCT states.[53]

2.1.6. Summary: Assignment of Excited States and Time Constants. The spectroscopic studies described here paint a fuller picture of the photophysics of Ni(^{R}bpy)(Ar)X. Beginning with light absorption, the complexes have a visible absorption band which is assigned as a MLCT transition. This is supported by the observation of bathochromic shifts as the bpy π^* is lowered or as the Ni-centered orbitals are raised.

After excitation at the MLCT band and vibrational relaxation, a MLCT state persists for ∼5−10 ps (Figure 10). The assignment of this species as MLCT is enabled by the observation of bpy radical anion signatures in the TA spectra. Further evidence is found in the reduction of the C═O stretching frequency, as measured by TRIR. The spin state of this species is currently not known experimentally.

The data suggest that the initially formed MLCT state evolves over ∼5−10 ps into a long-lived, tetrahedral ^{3}d-d state with a lifetime of ∼4 ns (∼7 ns for the Br-containing aryl series **2**).[54] The assignment of a tetrahedral ^{3}d-d state is supported by the following experimental data:

(1) Loss of a bpy$^{\bullet-}$ signature in TA, suggesting evolution away from an excited state of MLCT character,
(2) Little trend of excited state lifetime with MLCT energy, which is reasonable for an excited state that is not MLCT,
(3) Insensitivity of excited state lifetimes to solvent Lewis basicity, which suggests a tetrahedral (and thus d-d) state that is resistant to ligand binding,
(4) An increased C═O stretching frequency relative to the ground state, which rules out a reduced bpy ligand but is consistent with weakened π-backbonding in a d-d state,
(5) Dynamic *cis,trans*-isomerization, which involves twisting through a tetrahedral (and thus d-d) state.

The assignment of a triplet spin state is based on the comparatively long time constant associated with its decay, consistency of computed triplet states with experimental data, and precedence for tetrahedral triplet (i.e., high spin) states.

Through a combination of 2D EXSY and TA spectroscopy, the energy of the nonemissive ^{3}d-d state was determined. It was found to lie ∼0.5 eV (12 kcal/mol) above the ground state, rendering it thermally accessible at room temperature. *The low-energy ^{3}d-d state provides a mechanism for dynamic cis,trans-isomerization, which may have major implications for selectivity in Ni catalysis.*

Ultimately, the assignment of the longest-lived state as ^{3}d-d is in line with the photophysics of most first-row transition metal complexes.[23−25] As a result of the primogenic effect, d-orbital splittings tend to be small in first-row transition metals, often leading to the lowest excited states being d-d rather than charge transfer in nature.[55] Evidently, this remains true for Ni(^{R}bpy)(Ar)X, despite the presence of a strongly donating, carbanionic aryl ligand.

2.2. Mechanistic Implications for Ni-Photoredox. The assignment of the longest lived state as ^{3}d-d raises interesting mechanistic possibilities in the context of Ni-photoredox catalysis. This is because the ^{3}d-d (i.e., high spin) state has occupied metal−ligand σ^* orbitals (the t_2 set in idealized tetrahedral geometry, Figure 11A). The σ-antibonding character is clearly seen as nodes in the computed spin density and results in weakened metal−ligand bonds (Figure 11B). *Thus, we propose*

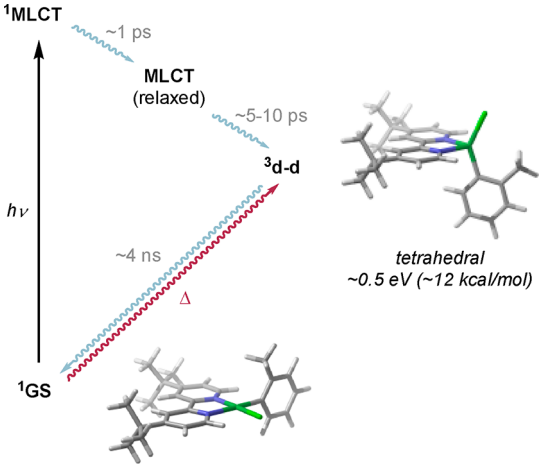

Figure 10. Relaxation pathway of Ni(^{R}bpy)(Ar)X following MLCT excitation, illustrated for the $^{t\text{-Bu}}$bpy variant (**1**$^{t\text{-Bu}}$). Structures shown were calculated by DFT (M06/TZVP//B3LYP/TZVP).

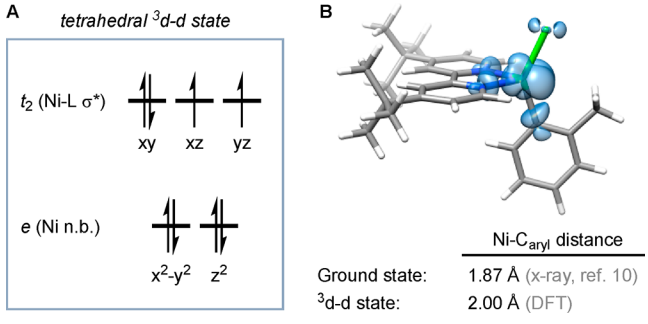

Figure 11. Bond weakening in the ^{3}d-d state. (A) Molecular orbital diagram of a high-spin Ni(II) center in idealized T_d symmetry. (B) Computed spin density and Ni−Ar distances.

https://dx.doi.org/10.1021/jacs.0c00781
J. Am. Chem. Soc. 2020, 142, 5800−5810

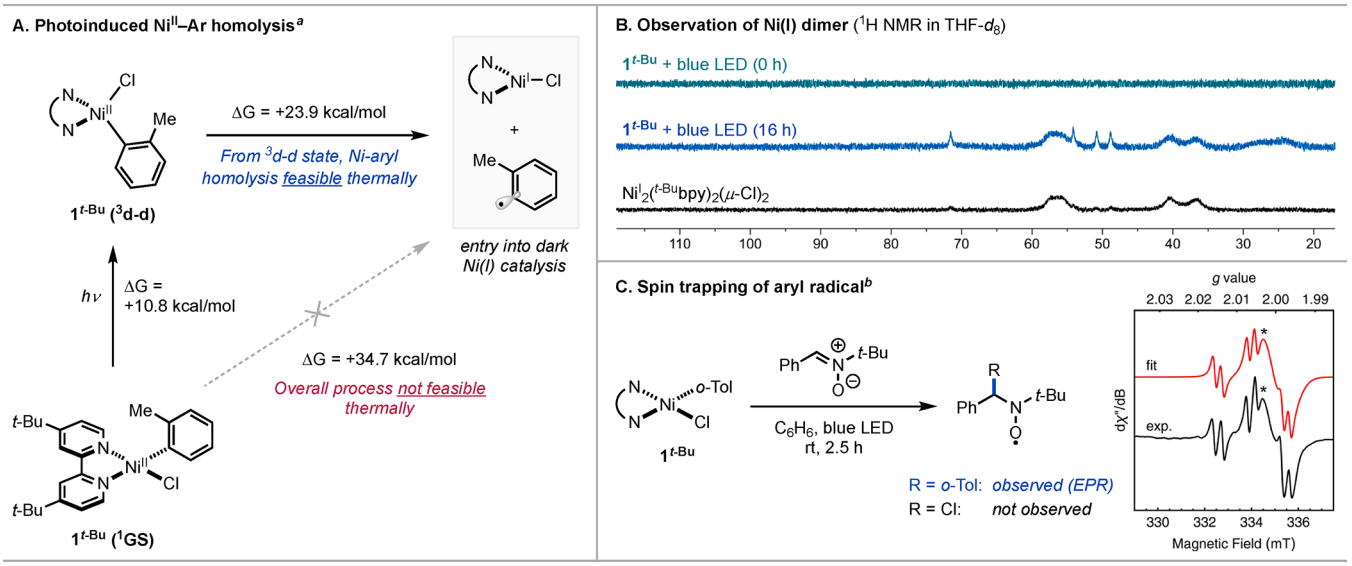

Figure 12. Generation of Ni(I) and aryl radicals through photoinduced Ni–Ar bond homolysis. [a]Free energies computed by DFT (M06/TZVP//B3LYP/TZVP). [b]EPR spectrum measured in C_6H_6 at room temperature. An unknown species (starred) overlaps with the spin adduct. Spectrum was fit to a sum of two components. Fit parameters for component 1: $g = 2.006$, $a_N = 40.5$ MHz, $a_H = 8.8$ MHz. Fit parameters for component 2 (starred): $g = 2.001$.

that photoinduced Ni(II)–Ar bond homolysis can occur through the ^{3}d-d state (Figure 12A).[56]

Photoinduced Ni–Ar homolysis would have major ramifications, as it generates an aryl radical and Ni(I). Since Ni(I) can thermally catalyze reactions proceeding via Ni(I)/Ni(III) cycles, light could serve as an initiator for catalysis that can occur in the dark. This concept of photoinitiated Ni(I) catalysis has been previously demonstrated, where Ni(I) was generated by electron transfer.[57] *Photoinduced Ni–Ar homolysis offers a unique mechanism of generating Ni(I) for catalysis.* Interestingly, this raises the possibility that cross-couplings proposed to proceed via photoinduced reductive elimination may operate via a photoinitiated Ni(I)/Ni(III) cycle.[8,53,57]

The feasibility of photoinduced Ni–Ar bond homolysis is supported both computationally and experimentally. DFT calculations predict the Ni–Ar bond to be very weak in the ground state (bond dissociation free energy (BDFE) = 34.7 kcal/mol). A bond of this strength would be stable at ambient temperature but could spontaneously homolyze when starting from a ^{3}d-d state that is 10.8 kcal/mol higher in energy.[58] While the *individual* steps of accessing the ^{3}d-d state and the subsequent Ni–Ar homolysis are both thermally feasible, the *sum* of the steps is not and requires the input of light energy.[59] Thus, light could generate the ^{3}d-d state, which then undergoes thermal homolysis of the Ni–Ar bond. The Ni–halogen bond is computed to be too strong to photolyze in the Ni(II) oxidation state (ground state BDFE: Ni–Cl = 76.8 kcal/mol, Ni–Br = 63.3 kcal/mol; Figures S55 and S56).

With computational support for the feasibility of photoinduced Ni–Ar homolysis, we sought experimental evidence for the photogeneration of Ni(I) and aryl radicals. Ni(I) was directly observed by ^{1}H NMR upon exposure of $\mathbf{1}^{t\text{-Bu}}$ to blue light (Figure 12B). Peaks in the paramagnetic region were observed that were consistent with independently prepared Ni(I) dimer $Ni^I_2(^{t\text{-Bu}}bpy)_2(\mu\text{-Cl})_2$.[60] Notably, Ni–Ar homolysis would initially generate Ni(I) in a more reactive monomeric form that may not be accessible by comproportionation, which unites two Ni complexes in a single transition state.

To establish the formation of aryl radicals, a spin-trapping experiment was done by irradiating $\mathbf{1}^{t\text{-Bu}}$ in the presence of *N-tert*-butyl-α-phenylnitrone (PBN). The spin adduct of the *o*-tolyl radical was observed by electron paramagnetic resonance (EPR) spectroscopy as a diagnostic triplet of doublets resulting from hyperfine coupling to the ^{14}N and ^{1}H nuclei (Figure 12C).[61] This signal is overlapped with an unidentified singlet (starred), which is not observed when irradiating $\mathbf{1}^{t\text{-Bu}}$ alone and is thus ascribed to downstream reactivity involving PBN (Figure S39). Thus, we obtained evidence for the generation of both species that would result from photoinduced Ni–Ar homolysis (the fate of the aryl radical is discussed in the Supporting Information, see Figure S40). We note that trapping of Cl$^\bullet$ radical with PBN was not observed, as the Cl$^\bullet$ adduct exhibits additional quartet splitting in the EPR spectrum (^{35,37}Cl both spin 3/2).[62] The absence of chlorine radical trapping argues against photoinduced Ni(II)–Cl homolysis and a previously proposed photoinduced disproportionation.[10] Disproportionation would form a Ni(III) species that extrudes Cl$^\bullet$ under irradiation.[63−65] Moreover, a photoinduced disproportionation would be highly endergonic (by ∼1.5 V or 34 kcal/mol) if starting from a ^{3}d-d state that is 1.1 eV lower in energy than the previously computed ^{3}MLCT state.[10] Such a process would not be energetically feasible, supporting that Ni–Ar homolysis from the ^{3}d-d state is a more likely process.

While this study identifies a new pathway available to excited Ni(II) complexes, many questions remain to be answered. For instance, it is difficult to establish what the predominant mechanism is in a catalytic reaction, which likely contains a mixture of multiple Ni species that absorb visible light. Furthermore, it is unclear why some reactions proceeding through excited Ni(II) require an exogenous photocatalyst while others do not. Nonetheless, photoinduced Ni–Ar homolysis unlocks exciting possibilities to develop Ni-catalyzed reactions that are driven by light but do not require exogenous photocatalysts.

https://dx.doi.org/10.1021/jacs.0c00781
J. Am. Chem. Soc. 2020, 142, 5800−5810

3. CONCLUSION

In summary, complexes of the general type Ni(^{R}bpy)(Ar)X have been studied spectroscopically in order to characterize their excited states. The complexes have a MLCT absorption band in the visible region, and experimental evidence suggests that excitation at this band generates a MLCT state that rapidly decays into a long-lived ^{3}d-d state. We therefore revise the prior assignment of a long-lived MLCT state from two of our groups. The ^{3}d-d state identified in this study is believed to be tetrahedral and ∼12 kcal/mol (0.5 eV) above the ground state. Moreover, it is thermally accessible at ambient temperature and gives rise to dynamic *cis*,*trans*-isomerization. We propose that the weakened bonds of the ^{3}d-d state provide a pathway for photoinduced homolysis of the Ni(II)−aryl bond, generating an aryl radical and Ni(I), both of which are corroborated experimentally. In the context of catalytic reactions, light may thus serve to initiate a dark catalytic cycle based on Ni(I). These findings may inform the development of Ni-catalyzed reactions that do not rely on exogenous photocatalysts.

■ ASSOCIATED CONTENT

Supporting Information

The Supporting Information is available free of charge at https://pubs.acs.org/doi/10.1021/jacs.0c00781.

Experimental procedures, experimental and computational data, and characterization and spectral data for new compounds (PDF)

■ AUTHOR INFORMATION

Corresponding Author

Abigail G. Doyle − *Department of Chemistry, Princeton University, Princeton, New Jersey 08544, United States;* orcid.org/0000-0002-6641-0833; Email: agdoyle@princeton.edu

Authors

Stephen I. Ting − *Department of Chemistry, Princeton University, Princeton, New Jersey 08544, United States;* orcid.org/0000-0002-6146-8112

Sofia Garakyaraghi − *Department of Chemistry, Princeton University, Princeton, New Jersey 08544, United States*

Chelsea M. Taliaferro − *Department of Chemistry, North Carolina State University, Raleigh, North Carolina 27695-8204, United States*

Benjamin J. Shields − *Department of Chemistry, Princeton University, Princeton, New Jersey 08544, United States*

Gregory D. Scholes − *Department of Chemistry, Princeton University, Princeton, New Jersey 08544, United States;* orcid.org/0000-0003-3336-7960

Felix N. Castellano − *Department of Chemistry, North Carolina State University, Raleigh, North Carolina 27695-8204, United States;* orcid.org/0000-0001-7546-8618

Complete contact information is available at: https://pubs.acs.org/10.1021/jacs.0c00781

Notes

The authors declare no competing financial interest.

■ ACKNOWLEDGMENTS

We thank Dr. István Pelczer for assistance with 2D EXSY, Dr. Talia J. Steiman, Bryan Kudisch, and Dr. Hannah J. Sayre for helpful discussions, Dan Oblinsky for assistance with transient absorption spectroscopy, and Dr. Jacob Sanders for assistance with computations. Financial support for this project was provided by the BioLEC, an Energy Frontier Research Center funded by the U.S. Department of Energy, Office of Science, Office of Basic Energy Sciences under Award no. DE-SC0019370.

■ REFERENCES

(1) Twilton, J.; Le, C.; Zhang, P.; Shaw, M. H.; Evans, R. W.; MacMillan, D. W. C. The Merger of Transition Metal and Photocatalysis. *Nat. Rev. Chem.* **2017**, *1*, 0052.

(2) Milligan, J. A.; Phelan, J. P.; Badir, S. O.; Molander, G. A. Alkyl Carbon−Carbon Bond Formation by Nickel/Photoredox Cross-Coupling. *Angew. Chem., Int. Ed.* **2019**, *58*, 6152−6163.

(3) Narayanam, J. M. R.; Stephenson, C. R. J. Visible Light Photoredox Catalysis: Applications in Organic Synthesis. *Chem. Soc. Rev.* **2011**, *40*, 102−113.

(4) Prier, C. K.; Rankic, D. A.; MacMillan, D. W. C. Visible Light Photoredox Catalysis with Transition Metal Complexes: Applications in Organic Synthesis. *Chem. Rev.* **2013**, *113*, 5322−5363.

(5) Koike, T.; Akita, M. Visible-Light Radical Reaction Designed by Ru- and Ir-Based Photoredox Catalysis. *Inorg. Chem. Front.* **2014**, *1*, 562−576.

(6) Shaw, M. H.; Twilton, J.; MacMillan, D. W. C. Photoredox Catalysis in Organic Chemistry. *J. Org. Chem.* **2016**, *81*, 6898−6926.

(7) Heitz, D. R.; Tellis, J. C.; Molander, G. A. Photochemical Nickel-Catalyzed C−H Arylation: Synthetic Scope and Mechanistic Investigations. *J. Am. Chem. Soc.* **2016**, *138*, 12715−12718.

(8) Welin, E. R.; Le, C.; Arias-Rotondo, D. M.; McCusker, J. K.; MacMillan, D. W. C. Photosensitized, Energy Transfer-Mediated Organometallic Catalysis through Electronically Excited Nickel(II). *Science* **2017**, *355*, 380−385.

(9) Kudisch, M.; Lim, C.-H.; Thordarson, P.; Miyake, G. M. Energy Transfer to Ni-Amine Complexes in Dual Catalytic, Light-Driven C−N Cross-Coupling Reactions. *J. Am. Chem. Soc.* **2019**, *141*, 19479−19486.

(10) Shields, B. J.; Kudisch, B.; Scholes, G. D.; Doyle, A. G. Long-Lived Charge-Transfer States of Nickel(II) Aryl Halide Complexes Facilitate Bimolecular Photoinduced Electron Transfer. *J. Am. Chem. Soc.* **2018**, *140*, 3035−3039.

(11) Shen, X.; Li, Y.; Wen, Z.; Cao, S.; Hou, X.; Gong, L. A Chiral Nickel DBFOX Complex as a Bifunctional Catalyst for Visible-Light-Promoted Asymmetric Photoredox Reactions. *Chem. Sci.* **2018**, *9*, 4562−4568.

(12) Lim, C. H.; Kudisch, M.; Liu, B.; Miyake, G. M. C−N Cross-Coupling via Photoexcitation of Nickel−Amine Complexes. *J. Am. Chem. Soc.* **2018**, *140*, 7667−7673.

(13) Kim, D.; Holten, D. Picosecond Measurements on the Binding and Release of Basic Ligands by Excited States of Ni(II) Porphyrins. *Chem. Phys. Lett.* **1983**, *98*, 584−589.

(14) Kim, D.; Kirmaier, C.; Holten, D. Nickel Porphyrin Photophysics and Photochemistry. A Picosecond Investigation of Ligand Binding and Release in the Excited State. *Chem. Phys.* **1983**, *75*, 305−322.

(15) Drain, C. M.; Gentemann, S.; Roberts, J. A.; Nelson, N. Y.; Medforth, C. J.; Jia, S.; Simpson, M. C.; Smith, K. M.; Fajer, J.; Shelnutt, J. A.; Holten, D. Picosecond to Microsecond Photodynamics of a Nonplanar Nickel Porphyrin: Solvent Dielectric and Temperature Effects. *J. Am. Chem. Soc.* **1998**, *120*, 3781−3791.

(16) Chen, L. X.; Zhang, X.; Wasinger, E. C.; Attenkofer, K.; Jennings, G.; Muresan, A. Z.; Lindsey, J. S. Tracking Electrons and Atoms in a Photoexcited Metalloporphyrin by X-Ray Transient Absorption Spectroscopy. *J. Am. Chem. Soc.* **2007**, *129*, 9616−9618.

(17) Shelby, M. L.; Lestrange, P. J.; Jackson, N. E.; Haldrup, K.; Mara, M. W.; Stickrath, A. B.; Zhu, D.; Lemke, H. T.; Chollet, M.; Hoffman, B. M.; Li, X.; Chen, L. X. Ultrafast Excited State Relaxation of a Metalloporphyrin Revealed by Femtosecond X-Ray Absorption Spectroscopy. *J. Am. Chem. Soc.* **2016**, *138*, 8752−8764.

(18) Hong, J.; Kelley, M. S.; Shelby, M. L.; Hayes, D. K.; Hadt, R. G.; Rimmerman, D.; Zhang, X.; Chen, L. X. The Nature of the Long-Lived

Excited State in a Ni^{II} Phthalocyanine Complex Investigated by X-Ray Transient Absorption Spectroscopy. *ChemSusChem* **2018**, *11*, 2421−2428.
(19) Campagna, S.; Puntoriero, F.; Nastasi, F.; Bergamini, G.; Balzani, V. Photochemistry and Photophysics of Coordination Compounds: Ruthenium. *Top. Curr. Chem.* **2007**, *280*, 117−214.
(20) Durham, B.; Caspar, J. V.; Nagle, J. K.; Meyer, T. J. Photochemistry of $Ru(bpy)_3^{2+}$. *J. Am. Chem. Soc.* **1982**, *104*, 4803−4810.
(21) Caspar, J. V.; Meyer, T. J. Photochemistry of $Ru(bpy)_3^{2+}$. Solvent Effects. *J. Am. Chem. Soc.* **1983**, *105*, 5583−5590.
(22) Pal, A. K.; Hanan, G. S. Design, Synthesis and Excited-State Properties of Mononuclear Ru(II) Complexes of Tridentate Heterocyclic Ligands. *Chem. Soc. Rev.* **2014**, *43*, 6184−6197.
(23) Liu, Y.; Persson, P.; Sundström, V.; Wärnmark, K. Fe *N*-Heterocyclic Carbene Complexes as Promising Photosensitizers. *Acc. Chem. Res.* **2016**, *49*, 1477−1485.
(24) Larsen, C. B.; Wenger, O. S. Photoredox Catalysis with Metal Complexes Made from Earth-Abundant Elements. *Chem. - Eur. J.* **2018**, *24*, 2039−2058.
(25) Wenger, O. S. Photoactive Complexes with Earth-Abundant Metals. *J. Am. Chem. Soc.* **2018**, *140*, 13522−13533.
(26) Both series have OMe as the most electron-donating substituent (σ_p = −0.27, ref 27).
(27) Hansch, C.; Leo, A.; Taft, R. W. A Survey of Hammett Substituent Constants and Resonance and Field Parameters. *Chem. Rev.* **1991**, *91*, 165−195.
(28) Murrell, J. N. The Theory of Charge-Transfer Spectra. *Q. Rev., Chem. Soc.* **1961**, *15*, 191−206.
(29) Phifer, C. C.; McMillin, D. R. The Basis of Aryl Substituent Effects on Charge-Transfer Absorption Intensities. *Inorg. Chem.* **1986**, *25*, 1329−1333.
(30) Braterman, P. S.; Song, J.-I. Spectroelectrochemistry of Aromatic Ligands and Their Derivatives. 1. Reduction Products of 4,4′-Bipyridine, 2,2′-Bipyridine, 2,2′-Bipyrimidine, and Some Quaternized Derivatives. *J. Org. Chem.* **1991**, *56*, 4678−4682.
(31) Yoshimura, A.; Hoffman, M. Z.; Sun, H. An Evaluation of the Excited State Absorption Spectrum of $Ru(bpy)_3^{2+}$ in Aqueous and Acetonitrile Solutions. *J. Photochem. Photobiol., A* **1993**, *70*, 29−33.
(32) Juban, E. A.; McCusker, J. K. Ultrafast Dynamics of 2E State Formation in $Cr(acac)_3$. *J. Am. Chem. Soc.* **2005**, *127*, 6857−6865.
(33) Brown, A. M.; McCusker, C. E.; Carey, M. C.; Blanco-Rodríguez, A. M.; Towrie, M.; Clark, I. P.; Vlček, A.; McCusker, J. K. Vibrational Relaxation and Redistribution Dynamics in Ruthenium(II) Polypyridyl-Based Charge-Transfer Excited States: A Combined Ultrafast Electronic and Infrared Absorption Study. *J. Phys. Chem. A* **2018**, *122*, 7941−7953.
(34) The persistence of ESA1 could also be explained by a ^{3}MLCT state (ref 10). Regarding ESA2, both a ^{3}MLCT state and a ^{3}d-d state are computed to absorb at 600 nm (with similar extinction coefficients). The ^{3}MLCT state, however, has a ∼5-fold higher extinction coefficient at 700 nm. See ref 10 and Figure S50.
(35) Kober, E. M.; Caspar, J. V.; Lumpkin, R. S.; Meyer, T. J. Application of the Energy Gap Law to Excited-State Decay of Osmium(II)-Polypyridine Complexes: Calculation of Relative Nonradiative Decay Rates from Emission Spectral Profiles. *J. Phys. Chem.* **1986**, *90*, 3722−3734.
(36) Williams, J. A. G. Photochemistry and Photophysics of Coordination Compounds: Platinum. *Top. Curr. Chem.* **2007**, *281*, 205−268.
(37) Crites Tears, D. K.; McMillin, D. R. Exciplex Quenching of Photoexcited Platinum(II) Terpyridines: Influence of the Orbital Parentage. *Coord. Chem. Rev.* **2001**, *211*, 195−205.
(38) Ichinaga, A. K.; Kirchhoff, J. R.; McMillin, D. R.; Dietrich-Buchecker, C. O.; Marnot, P. A.; Sauvage, J. P. Charge-Transfer Absorption and Emission of $Cu(NN)_2^+$ Systems. *Inorg. Chem.* **1987**, *26*, 4290−4292.
(39) Armaroli, N. Photoactive Mono- and Polynuclear Cu(I)−Phenanthrolines. A Viable Alternative to Ru(II)−Polypyridines? *Chem. Soc. Rev.* **2001**, *30*, 113−124.
(40) Mara, M. W.; Fransted, K. A.; Chen, L. X. Interplays of Excited State Structures and Dynamics in Copper(I) Diimine Complexes: Implications and Perspectives. *Coord. Chem. Rev.* **2015**, *282*−*283*, 2−18.
(41) Hong, J.; Fauvell, T. J.; Helweh, W.; Zhang, X.; Chen, L. X. Investigation of the Photoinduced Axial Ligation Process in the Excited State of Nickel(II) Phthalocyanine. *J. Photochem. Photobiol., A* **2019**, *372*, 270−278.
(42) Gutmann, V. Solvent Effects on the Reactivities of Organometallic Compounds. *Coord. Chem. Rev.* **1976**, *18*, 225−255.
(43) Benzene and THF are similar in viscosity. Benzene: 0.65 cP. THF: 0.55 cP.
(44) Klein, A.; Kaiser, A.; Wielandt, W.; Belaj, F.; Wendel, E.; Bertagnolli, H.; Záliš, S. Halide Ligands − More Than Just σ-Donors? A Structural and Spectroscopic Study of Homologous Organonickel Complexes. *Inorg. Chem.* **2008**, *47*, 11324−11333.
(45) Feth, M. P.; Klein, A.; Bertagnolli, H. Investigation of the Ligand Exchange Behavior of Square-Planar Nickel(II) Complexes by X-ray Absorption Spectroscopy and X-ray Diffraction. *Eur. J. Inorg. Chem.* **2003**, *2003*, 839−852.
(46) For overlays of normalized kinetic traces, see Supporting Information.
(47) Balzani, V.; Carassiti, V. Photochemistry of Some Square-Planar and Octahedral Platinum Complexes. *J. Phys. Chem.* **1968**, *72*, 383−388.
(48) Goodgame, D. M. L.; Goodgame, M.; Cotton, F. A. Electronic Spectra of Some Tetrahedral Nickel(II) Complexes. *J. Am. Chem. Soc.* **1961**, *83*, 4161−4167.
(49) Schumann, M.; Elias, H. Kinetics and Mechanism of Ligand Substitution in Four-Coordinate Nickel(II) Chelate Complexes: Study on the Reactivities of Planar and Tetrahedral Configurational Isomers and Octahedral Adducts. *Inorg. Chem.* **1985**, *24*, 3187−3192.
(50) Knoch, R.; Elias, H.; Paulus, H. Configurational Isomerism in Bis(*N*-alkylsalicylaldiminato)nickel(II) Complexes: The Equilibrium Planar ⇌ Tetrahedral and Its Effect on the Kinetics and Mechanism of Ligand Substitution. *Inorg. Chem.* **1995**, *34*, 4032−4040.
(51) McCusker, C. E.; Castellano, F. N. Design of a Long-Lifetime, Earth-Abundant, Aqueous Compatible Cu(I) Photosensitizer Using Cooperative Steric Effects. *Inorg. Chem.* **2013**, *52*, 8114−8120.
(52) Perrin, C. L.; Dwyer, T. J. Application of Two-Dimensional NMR to Kinetics of Chemical Exchange. *Chem. Rev.* **1990**, *90*, 935−967.
(53) Ma, P.; Wang, S.; Chen, H. Reactivity of Transition-Metal Complexes in Excited States: C−O Bond Coupling Reductive Elimination of a Ni(II) Complex Is Elicited by the Metal-to-Ligand Charge Transfer State. *ACS Catal.* **2020**, *10*, 1−6.
(54) A previous study by two of our groups implicated exciplex formation based on the effect of Ni complex concentration on excited state lifetime (ref 10). However, a tetrahedral ^{3}d-d state supported by the present study suggests that exciplex formation via interaction with the d_{z^2} orbital would not be possible; we are currently unsure how to reconcile these findings.
(55) McCusker, J. K. Electronic Structure in the Transition Metal Block and Its Implications for Light Harvesting. *Science* **2019**, *363*, 484−488.
(56) A related photoinduced Ni(II)−CH_3 homolysis is known: Lapointe, S.; Khaskin, E.; Fayzullin, R. R.; Khusnutdinova, J. R. Nickel(II) Complexes with Electron-Rich, Sterically Hindered PNP Pincer Ligands Enable Uncommon Modes of Ligand Dearomatization. *Organometallics* **2019**, *38*, 4433−4447.
(57) Sun, R.; Qin, Y.; Ruccolo, S.; Schnedermann, C.; Costentin, C.; Nocera, D. G. Elucidation of a Redox-Mediated Reaction Cycle for Nickel-Catalyzed Cross Coupling. *J. Am. Chem. Soc.* **2019**, *141*, 89−93.
(58) The Ni−Ar BDFE in the ^{3}d-d state is 23.8 kcal/mol. While we were unable to locate a transition state for this homolysis, DFT suggests that the free energy barrier has a similar value, as no electronic energy maximum is passed during bond homolysis (i.e., $\Delta E^{\ddagger} = \Delta E$, Figure

https://dx.doi.org/10.1021/jacs.0c00781
J. Am. Chem. Soc. 2020, 142, 5800−5810

S54). Based on the Eyring equation, a $\Delta G^{\ddagger}$ of 23.8 kcal/mol falls below the ~25 kcal/mol threshold for barriers that are surmountable at room temperature.

(59) The *overall* process of accessing the ^{3}d-d state and homolyzing the Ni−Ar bond requires surmounting an energetic barrier of ~35 kcal/mol. Based on the Eyring equation, such a barrier requires temperatures of ~150 °C to be overcome on a reasonable time scale ($t_{1/2} \approx 1$ day). At room temperature, a barrier of 35 kcal/mol corresponds to a half-life of ~10^5 years.

(60) Mohadjer Beromi, M.; Brudvig, G. W.; Hazari, N.; Lant, H. M. C.; Mercado, B. Q. Synthesis and Reactivity of Paramagnetic Nickel Polypyridyl Complexes Relevant to C(sp^2)-C(sp^3)Coupling Reactions. *Angew. Chem., Int. Ed.* **2019**, *58*, 6094−6098.

(61) Kamimori, M.; Sakuragi, H.; Suehiro, T.; Tokumaru, K.; Yoshida, M. Spin Trapping of Aryl and Arylcyclohexadienyl Radicals by *N*-*t*-Butyl-α-phenylnitrone (*N*-Benzylidene-*t*-butylamine Oxide) and α,*N*-Diphenylnitrone (*N*-Benzylideneaniline Oxide). *Bull. Chem. Soc. Jpn.* **1977**, *50*, 1195−1200.

(62) Janzen, E. G.; Knauer, B. R.; Williams, L. T.; Harrison, W. B. Electron Spin Resonance of β-Chloroalkyl Nitroxides. Angular Dependence of β-Chlorine Hyperfine Coupling. *J. Phys. Chem.* **1970**, *74*, 3025−3027.

(63) Shields, B. J.; Doyle, A. G. Direct C(sp^3)−H Cross Coupling Enabled by Catalytic Generation of Chlorine Radicals. *J. Am. Chem. Soc.* **2016**, *138*, 12719−12722.

(64) Hwang, S. J.; Powers, D. C.; Maher, A. G.; Anderson, B. L.; Hadt, R. G.; Zheng, S.-L.; Chen, Y.-S.; Nocera, D. G. Trap-Free Halogen Photoelimination from Mononuclear Ni(III) Complexes. *J. Am. Chem. Soc.* **2015**, *137*, 6472−6475.

(65) Hwang, S. J.; Anderson, B. L.; Powers, D. C.; Maher, A. G.; Hadt, R. G.; Nocera, D. G. Halogen Photoelimination from Monomeric Nickel(III) Complexes Enabled by the Secondary Coordination Sphere. *Organometallics* **2015**, *34*, 4766−4774.

https://dx.doi.org/10.1021/jacs.0c00781
J. Am. Chem. Soc. 2020, 142, 5800−5810